Sensors & Actuators: A. Physical 343 (2022) 113671

Contents lists available at ScienceDirect

Sensors and Actuators: A. Physical

journal homepage: www.journals.elsevier.com/sensors-and-actuators-a-physical

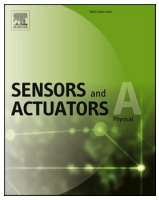

A microsensor array for diesel engine lubricant monitoring using deep learning with stochastic global optimization

Aaron Urban, Jiang Zhe *

Department of Mechanical Engineering, The University of Akron, 244 Sumner Street, Akron, OH 44325–3903, United States

ARTICLE INFO

Keywords:
Lubrication oil
Sensor array
Condition monitoring
Temperature compensation, Neural network

ABSTRACT

Measurement of concentrations of the critical properties in a diesel powered machine's lubricant oil is an important task in preventing machine failure and excessive damage. While there are several existing sensors for detecting these properties individually, they suffer from cross sensitivity issues and tedious calibrations for varying operating temperatures. We developed an interdigital sensor array based on an artificial neural network (ANN) automatically tuned with a stochastic global optimization (SGO) method for measuring water, base, soot, and diesel fuel contaminant concentrations in a lubricant oil. The temperature effect was compensated with the neural network. The neural network architecture was automatically selected through a unique simulated annealing process which resulted in an increased prediction accuracy when compared to the ANN with traditionally selected architecture. Dropout and data augmentation techniques were used during training to prevent overfitting. Experiment results demonstrated the ANN's ability in accurately determining the oil properties from the overlapped sensor responses as well as removing the need to calibrate for a variety of operating temperatures. The sensor array is able to provide comprehensive information about a diesel powered machine's health status.

1. Introduction

Diesel engines or diesel powered machines are widely used in construction, transportation, and agriculture industries [1]. Proper lubrication is critical to maintain the functionality of these engines/machines. Online monitoring the condition of the lubricants of diesel machines can help monitor the machine's health status, significantly reduce the maintenance cost and the unnecessary downtime, extend the life cycle and avoid catastrophic machine failure [2,3].

Lubricants used in diesel powered machines are formulated differently as they are subjected to a different set of working conditions compared to lubricants used in other machines [4]. Traditional lubrication monitoring typically take the following measurements: 1) viscosity, an indicator of the overall health of a lubricant [5], 2) water content, to evaluate the risk of losing functionality and rust development [2,6], and 3) the total base number (TBN), to determine the likelihood of oxidation of the lubricant [7]. In addition to the above key parameters, soot particles are generated from the combustion process of a diesel engine, which can get into the lubricant. Soot has a variety of adverse effects to the functionality of the lubricant and can lead to severe engine wear and damage [8]. Diesel fuel may also leak to the lubricant which can cause fuel dilution, resulting in a lower lubricant viscosity [9]. Hence monitoring the above key parameters of lubricants (i.e. viscosity, water content, TBN, soot content, fuel contamination) are critical to judge the health status of the diesel machines. While viscosity can be measured independently, to date there is no instrument that can take accurate measurements of other key parameters online [5,10].

While the above parameters can be analyzed in laboratories, they are not suitable for live monitoring as the results will typically take over a week to be received. Many researches have utilized multiple sensors to measure the specific lubricant properties online. For example, Surface acoustic wave sensors were used for viscosity measurements [11,12]. Capacitive sensors were used in monitoring water, total acid number (TAN), sulfur, and soot contents [11,13]. Excluding viscosity, most property sensors are based on the electrochemical sensing; one major challenge of these sensors is their cross-sensitivity or response overlapping, i.e., a sensor designed to measure a target property also responds to other properties. In our previous work, we had utilized a general regression neural network (GRNN) to measure the water content, TAN, and TBN, with a maximum error of 15.7% for water content [14]. However, all measurements were done in a constant temperature; the mechanism is only valid at a constant temperature. In practice, the operating temperature of lubricants typically varies during machine use, which significantly affects sensor responses. If the temperature effect is

* Corresponding author.

https://doi.org/10.1016/j.sna.2022.113671
Received 11 April 2022; Received in revised form 25 May 2022; Accepted 6 June 2022
Available online 9 June 2022

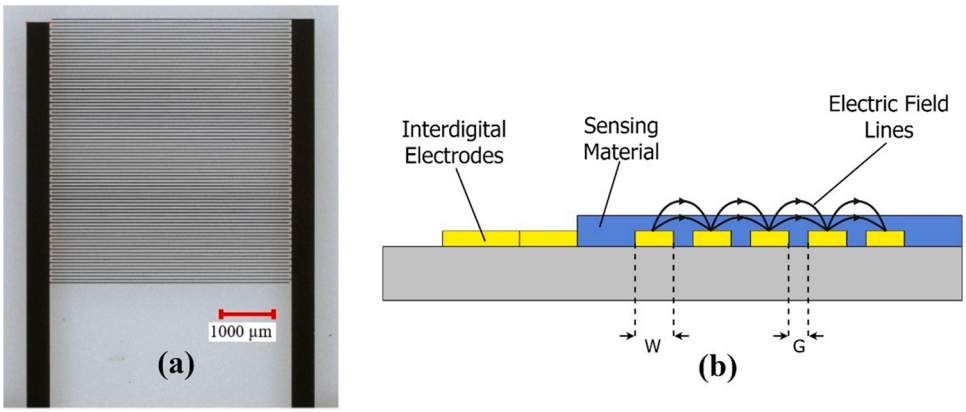

Fig. 1. a) Microscopic picture of Interdigital electrodes of the capacitive sensor, b) Side view of IDE sensor with sensing layer.

not accounted for, the measurements from the sensor array would be unreliable even if the ANN is used [15,16]. While calibration or training can be done at each temperature, the procedures are prohibitively tedious and time consuming if the temperature variation range is large.

Additionally, online machine health monitoring typically requires onsite training due to different operating conditions and the different base lubricants used in various machines [17]. The challenge is that it takes significant amount of time to prepare samples (or generating the datasets) for training. While a large size of samples/datasets usually improves the prediction accuracy, it is impractical to generate a large amount of samples on site. In the past decade, deep learning techniques have been used to improve the accuracy without a need of generating a large amount of samples. Among these techniques, data augmentation was used to increase the dataset size without compromising prediction accuracy. Recently, data augmentation has been used in several deep learning applications such as radio modulation classification, electroencephalography, and MRI reconstruction [18–20]. Dropout is a deep learning technique where nodes are randomly disabled during training, which greatly reduces overfitting issues in deep learning by preventing co-adaption among hidden nodes [21]. Dropout has shown effectiveness recently in credit card data analysis and ultrasonic flaw classification in weldments [22,23].

In this article, we present an interdigital micro sensor array for online monitoring of multiple properties of the diesel powered machines' lubricants based on a new artificial neural network with stochastic global optimization tuning. The new ANN used a unique stochastic global optimization (SGO) method, which allowed for the network to have higher prediction accuracy. Deep learning techniques including data augmentation and dropout were used to: 1) reduce the amount of the training samples, which is critical for onsite training, and 2) prevent overfitting during training to improve accuracy. The temperature is used as an input for the neural network to remove the temperature effect so that the sensor array can provide accurate measurement of lubricant properties at varying temperatures.

2. Material and methods

An array of four interdigital capacitive microsensors is designed to monitor the four critical properties (diesel fuel, water, base, and soot). Each microsensor consists of an identical pair of gold interdigitated electrodes (IDEs), and a specific sensing layer coated above the IDEs. By selecting a specific sensing layer, each of these four sensors responds primarily to one of these target properties with a larger weight ratio, while they may still respond to other properties with a smaller weight ratio. The IDEs were fabricated through a standard photolithography process, with 40 pairs of 5 mm fingers, a 25 µm finger width, and a 50 µm gap between fingers (see Fig. 1). Contents of water, acid, soot and fuel present in the lubricant are absorbed by the sensing layer, causing a change in the capacitance. Sensing layer thicknesses were selected to be smaller than W + G, where W is the IDE finger width, and G is the gap between the IDE fingers [11]. This selection was to ensure each sensor's response was dominated by the target property, but still influenced by other properties with a smaller weight ratio [24]. Fig. 1 shows a microscopic picture of the interdigital electrodes of the interdigital sensor. The coatings for the sensor which provide dominant sensitivity to one target properties are listed in Table 1. All coatings were applied by spin coating.

Table 1
Target properties and the selected sensing layers.

	Water	Base	Fuel contamination	Soot
Materials	PI-2545 polyimide	Nafion Dispersion	Tin Oxide Dispersion	None
Vendor	DuPont	Thermal Scientific	Thermal Scientific	N/A
Thickness	4 µm	250 nm	1 µm	N/A
Meas. Range	0–1000 ppm	0 – 2000 ppm	0 – 4000 ppm	0 – 4%

Polyimide (DuPont PI-2545) has proven to be effective in absorbing water, while preventing lubricant oil from being absorbed [25,26]. Nafion is commonly used in cation exchange membranes due to its ability to allow for the passage of positively charged ions, which make it excellent for sensing changes in the base content of a substance [14,27]. Tin Oxide (IV) has shown to be a good sensing layer for diesel contaminant sensors [28]. The soot sensor is a bare set of gold IDEs with no coating layer. Research shows that the amorphous carbon particles produced by incomplete combustion, adheres to gold electrodes easily, making it a suitable method for detecting soot. Each sensor's response is dominated by its target property, while content changes in other properties still have a small effect on the sensor response. The sensor responses were entered into a new ANN with SGO tuning to eliminate the cross sensitivity effect. Furthermore, since the capacitance of an IDE sensor is dependent on temperature, and the lubricant operating temperature of a machine is dynamic, we used a thermocouple to monitor the temperature of the lubricant. The temperature data was used in the neural network to correct any error in the sensor response which would be caused by temperature changes.

To train and validate the ANN, 64 samples containing varying concentrations of the four critical properties were prepared. A 10 W-30 synthetic grade lubricant for diesel engines (Grainger) was used as a base for all samples. Water levels of 500 ppm are known to be concerning, and concentrations of 1000 ppm are thought to be critical [6,29]. Water concentrations of 0 ppm, 500 ppm, and 1000 ppm were used in the training, which were modified by adding purified water to a sample. Base levels were modified by adding potassium hydroxide

(KOH). Base levels of 2000 ppm are thought to be alarming; thus, samples were prepared to concentrations of 0 ppm, 1000 ppm, and 2000 ppm [14]. A diesel fuel concentration of 2000 ppm is commonly accepted as a warning level, and 5000 ppm as an indicator for oil change [30]. Diesel concentrations of 0 ppm, 2000 ppm, and 5000 ppm were prepared to reflect these critical values and were altered by adding #2 grade diesel fuel. Soot concentration of 4% is considered to be dangerous [8]. Therefore, samples with soot concentrations of 0%, 2%, and 4% by adding carbon black. To remove the temperature influence, each sample was measured at a range of temperatures near their expected operating ranges, specifically at 90 C°, 100 C°, and 110 C° [31].

3. Theory

The neural network contains 5 inputs (4 from each of the 4 capacitive sensors, and 1 from a thermocouple) and 4 outputs (the contents of each property: water, base, diesel, and soot content). The neural network has many parameters which make up its architecture. These can be tuned to alter performance, including learning rate, optimization algorithm, the number of neurons in each layer, and the number of layers. To achieve highly accurate property predictions, we determined optimal network architecture using simulated annealing, which is a type of SGO [32,33]. Simulated annealing (SA) mimics the physical annealing process and is used for optimizing parameters in a neural network. This algorithm is proven useful for situations where there are a lot of local minima such that other algorithms (e.g. gradient descent) would be stuck at [34].

Using simulated annealing, an initial architecture was selected based on the number of input and output parameters in our network. The initial number of hidden neurons was selected as follows:

$$N = \frac{2}{3}I + O$$

where N is the number of hidden neurons, I is the number of input neurons, and O is the number of output neurons [35]. Following this criterion, we started with an architecture consisting of a single hidden layer with 7 neurons in it. The network had a learning rate of.01, and no extra hidden layers. We then defined a range of network architectures, with varied parameters of layers, neurons, and learning rates based on general guidelines [35,36]. The number of neurons in the first layer ranged from 5 to 15, the second layer from 0 to 11, and the third layer from 0 to 7. The learning rate ranged from 0.005 to 0.05.

Next, the simulated annealing algorithm automatically determined the optimal network architecture by comparing the performance of a neighboring architecture, which is an architecture that is similar except for a single parameter change. If the neighboring architecture increases the performance, it jumps to this architecture and compares the performance to another neighboring architecture. If the performance gets worse, it continues using the current set with a probability

$$P = e^{-[C(s')-C(s)]/kT}$$

where P is the probability it uses the current architecture, C(s′) is the cost of the neighboring architecture, C(s) is the cost of the current set of architecture, k is the Boltzmann constant, and T is a function which linearly decreases with each iteration [33]. The cost function is the root mean squared error for the property predictions. Once an architecture is selected, a single parameter is chosen at random and adjusted to another value within the predetermined ranges, with the following restrictions: 1) architectures could not be repeated, and 2) the number of neurons in the second and third layer could not be greater than the number of neurons in a previous layer. Simulated annealing allows for an extensive search of the solution space during the beginning of the search, allowing it to pass over local minimums. When the T function nears zero, the search converges on the global minimum. This final set of parameters was used as our network architecture, which will be discussed in the results section. The neural network and optimization were completed using Python and the Keras deep learning library.

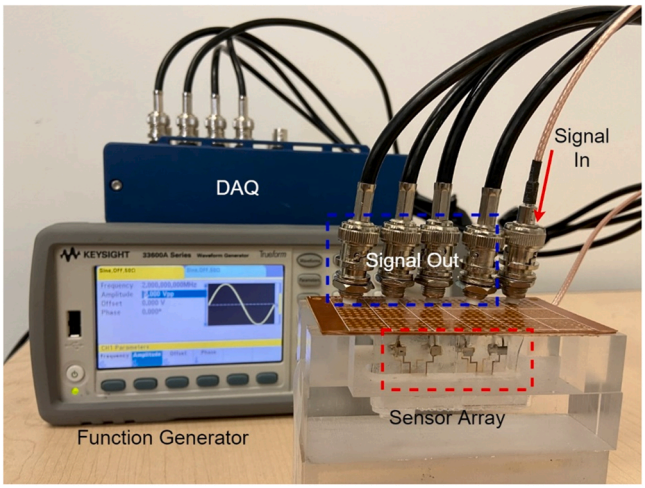

Fig. 2. Testing setup.

To avoid using a large amount of datasets, data augmentation was used to increase the dataset size with no need to generate a large amount of samples and without compromising prediction accuracy. The standard deviation of each sensor's response was calculated at steady state (t = 60 mins). Next, each sensor's noise was fit to a normal probability distribution. Values were probabilistically selected from this distribution, and these values were then added to each individual sample, resulting in an augmented data point [18]. The dataset was effectively doubled, from 192 samples to 384 samples with this method. This technique is known to prevent overfitting for datasets with limited data [18–20]. In addition, dropout was used to further increase the network performance. To implement the dropout technique, nodes were randomly disabled during each training iteration, which greatly reduced overfitting issues in deep learning [21,22]. For each iteration of training, every node in the hidden layers had a 10% chance of being disabled for that iteration, i.e., the node would be temporarily removed from the network and woulF55d not input or output data. This process helped prevent nodes from co-adapting, where they became too reliant or dependent on other nodes in the network [22].

4. Results and discussion

4.1. Sensor testing

The four sensors were immersed into an acrylic tank filled with oil samples with different water, diesel, base, and soot contents. The test setup is shown in Fig. 2, and is similar to that used in our prior publication. [14]. Static fluid conditions were used for the testing. It is worth mentioning that our prior research showed the responses of capacitive property sensors were in good agreement in both static and dynamic conditions [24]. The difference is that a hot plate (Thermo Fischer) was added to heat the oil samples to different temperatures (90 ℃, 100 ℃, and 110 ℃). Typical sensor responses to different samples as a function of time were plotted in Fig. 3. The sensor responses became stable at t = 60 min after immersion in the samples. Thus, the sensor response to each sample was collected at t = 60 min. The sensors were cleaned and dried before being tested in another sample.

Oil property changes cause changes in the dielectric constants of the sensing layer and the medium above the sensors and in turn causes capacitance changes of the sensors. The change in the capacitance of one sensor was measured in terms of a change of voltage across the sensor. A 2 MHz, 5 V_{pp}, sine wave excitation signal was applied to each sensor from an Agilent 33 600 A function generator. 2 MHz was selected as the excitation frequency because decent sensor responses were observed at

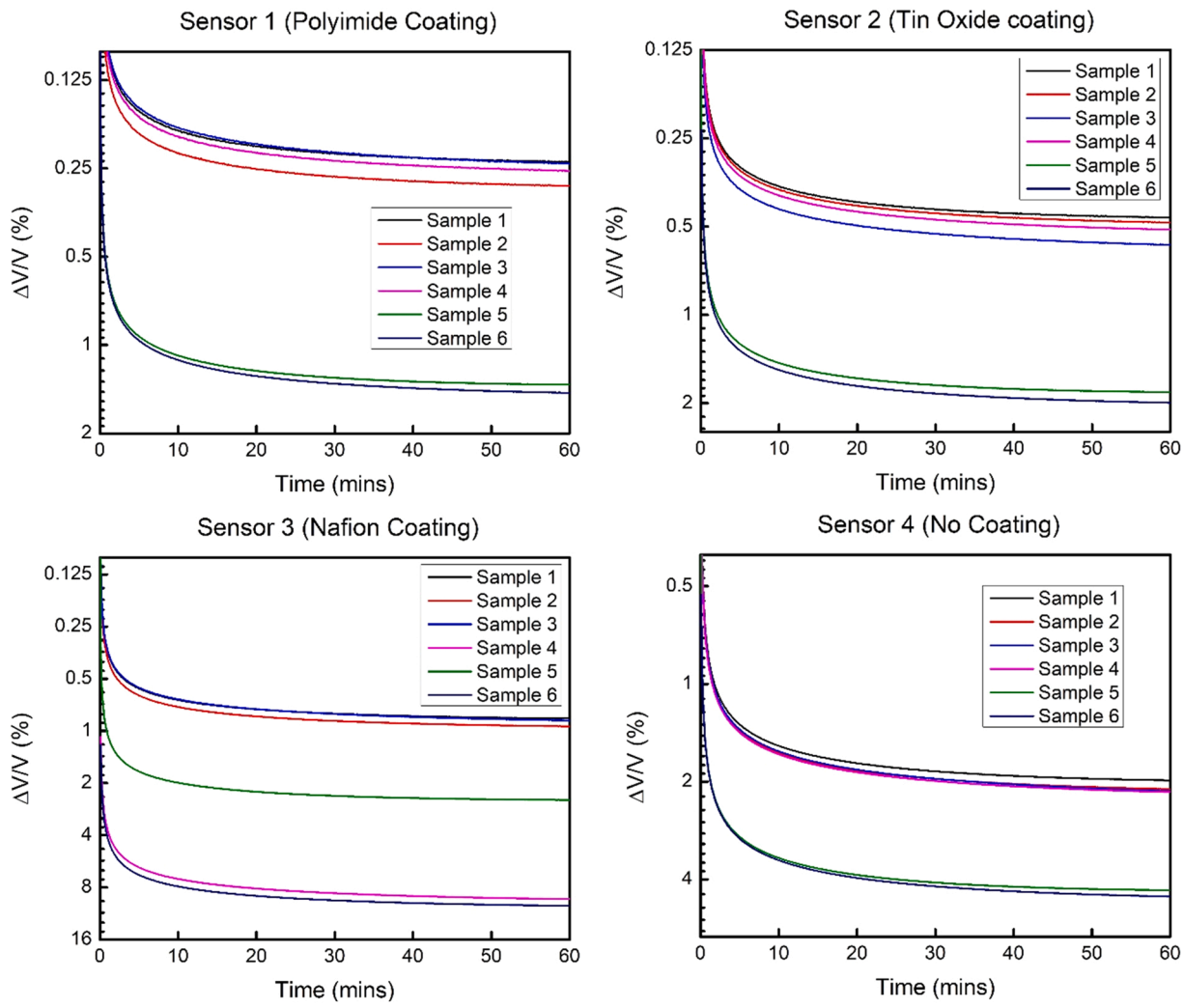

Fig. 3. Typical sensors' outputs from six samples. Sample 1: pure lubricant oil; Sample 2: 500 ppm water; Sample 3: 2000 ppm diesel; Sample 4: 1000 ppm base; Sample 5: 2% soot; Sample 6: 500 ppm water, 2000 ppm diesel, 1000 ppm base, 2% soot.

this frequency during a frequency sweep experiment. A rectifying circuit was placed into the measurement circuit so that the peak voltage values can be captured. The rectifying circuit took the sine wave signal from the sensor, and outputs the peak values to the DAQ. Voltage outputs from all sensors were recorded by an NI USB-6356 DAQ with a sampling rate of 60 Hz, using LabVIEW software.

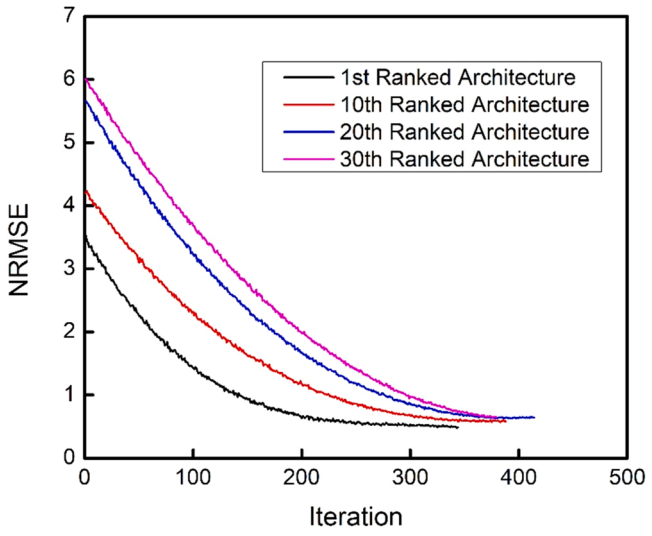

Fig. 4. Validation error vs. iteration for the 1st, 10th, 20th, and 30th ranked architectures.

The output of each sensor was analyzed in the frequency domain through a Fast Fourier Transform, and a bandpass filter was applied to remove unwanted noise present in the signal. A 10 s rolling average of the sensor was averaged to remove the remaining noise effect. The relative voltage change was then normalized to range from 0 to 1 as the inputs for the neural network.

4.2. *Neural network training*

After the dataset was increased with data augmentation, the 128 samples (each at 90 °C, 100 °C, and 110 °C), were used to train the network to minimize root mean square error (RMSE). 308 of the 384 datapoints were randomly selected to be the training set, and the remaining 76 were used as the validation set. After each training iteration, a k-fold cross validation method was used to select new validation and training sets to prevent overtraining. Starting with the initial architecture of a single layer with 7 neurons and a learning rate of.01, the neural network was trained until no property had a normalized root mean square error (NRMSE) greater than.08 in the validation set, and greater than.05 in the training set. A maximum of 500 iterations was set to prevent the code from getting stuck on a single architecture. This 500

Table 2
Parameters of architectures of the 1st, 10th, 20th, and 30th ranked architectures.

Rank	1st Layer Neurons	2nd Layer Neurons	3rd Layer Neurons	Learning Rate
1st	11	9	5	0.01
10th	13	7	5	0.01
20th	11	11	7	0.005
30th	15	3	3	0.01

iteration limit was selected based on the error vs. training iteration curves from our networks. Beyond this limit a majority of the networks training failed to reach our desired stopping conditions. Hidden neurons were randomly selected for dropout at each iteration with a dropout rate of 10%. Once the iterations were complete for the initial architecture, the training and validation errors were recorded. The neural network was trained with this neighboring architecture, and the errors of this network were compared to the previous architecture. The simulated annealing algorithm determined which of the two compared architectures would be used for the next step. The architecture selected by the algorithm then had one of its parameters modified, and the process was repeated. 100 architectures were analyzed through this process. For each architecture, a normalized RMSE (NRMSE) was calculated for each property by dividing the RMSE by the maximum concentration of that property. The sum of the NRMSE of the validation set of data was used as the metric to rank the architectures. The network which performed the best had 11 neurons in the first layer, 9 neurons in the second layer, 5 neurons in the third layer, and a learning rate of.01. This architecture was selected as the final set of network parameters. Fig. 4 shows the validation error as a function of training iteration number for the 1st, 10th, 20th, and 30th ranked architectures, and Table 2 shows the parameters of each architecture.

4.3. Neural network testing

Finally, a separate set of testing data containing 10 samples (each at 3 temperatures) which were unused in training and validation were used to evaluate the performance of the top 20 performing architectures, and to further ensure that the networks were not being overtrained. Fig. 5 shows the predictions of the 10 testing samples at 3 temperatures compared with the actual value for each sample. The average prediction for water, diesel, base and soot contents were 12.1%, 7.8%, 5.7%, and 3.9% respectively. The maximum prediction for these target properties were 15.2% (for water at 1000 ppm, 100 °C), 12.3% (for diesel at 5000 ppm, 100 °C), 6.7% (for base at 1500 ppm, 100 °C), and 3.7% (for soot at 2%, 90 °C). Water contained the largest maximum and average percent error, which was expected as the sensitivity of the polyimide sensor had the smallest sensitivity. Soot contained the smallest error, which was also expected since all of the sensors were more sensitive to changes in soot content than any other property. These errors are within industry guidelines for each property [8,30,37].

Predictions were also analyzed at different temperatures to see if the prediction errors were affected by temperature. The average error of each property was calculated for each temperature group to see if there was a correlation between temperature and error. There was an average testing error of 5.85%, 4.68%, and 6.04% at 90 °C, 100 °C, and 110 °C

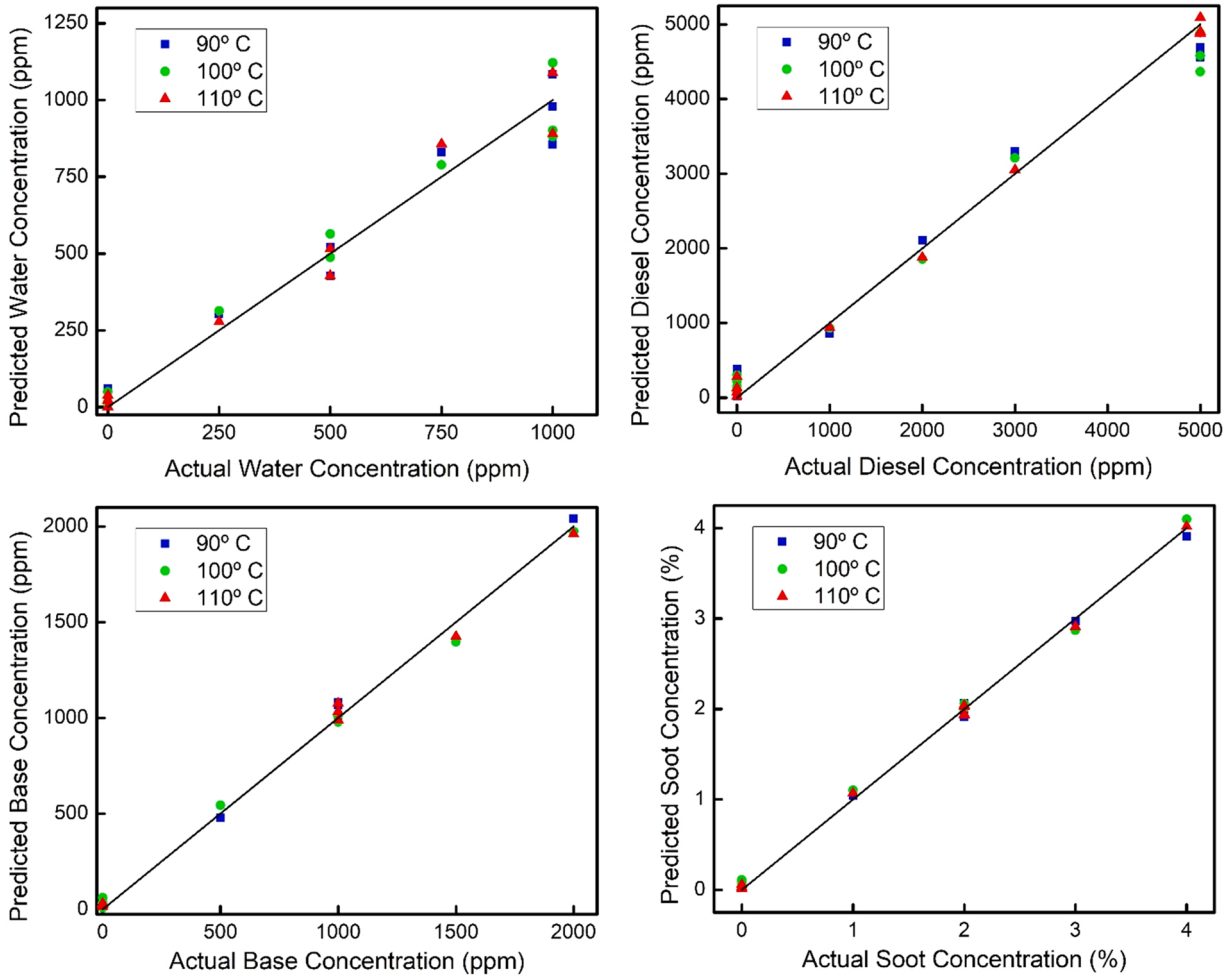

Fig. 5. Predicted concentration vs actual concentration of test samples at different temperatures.

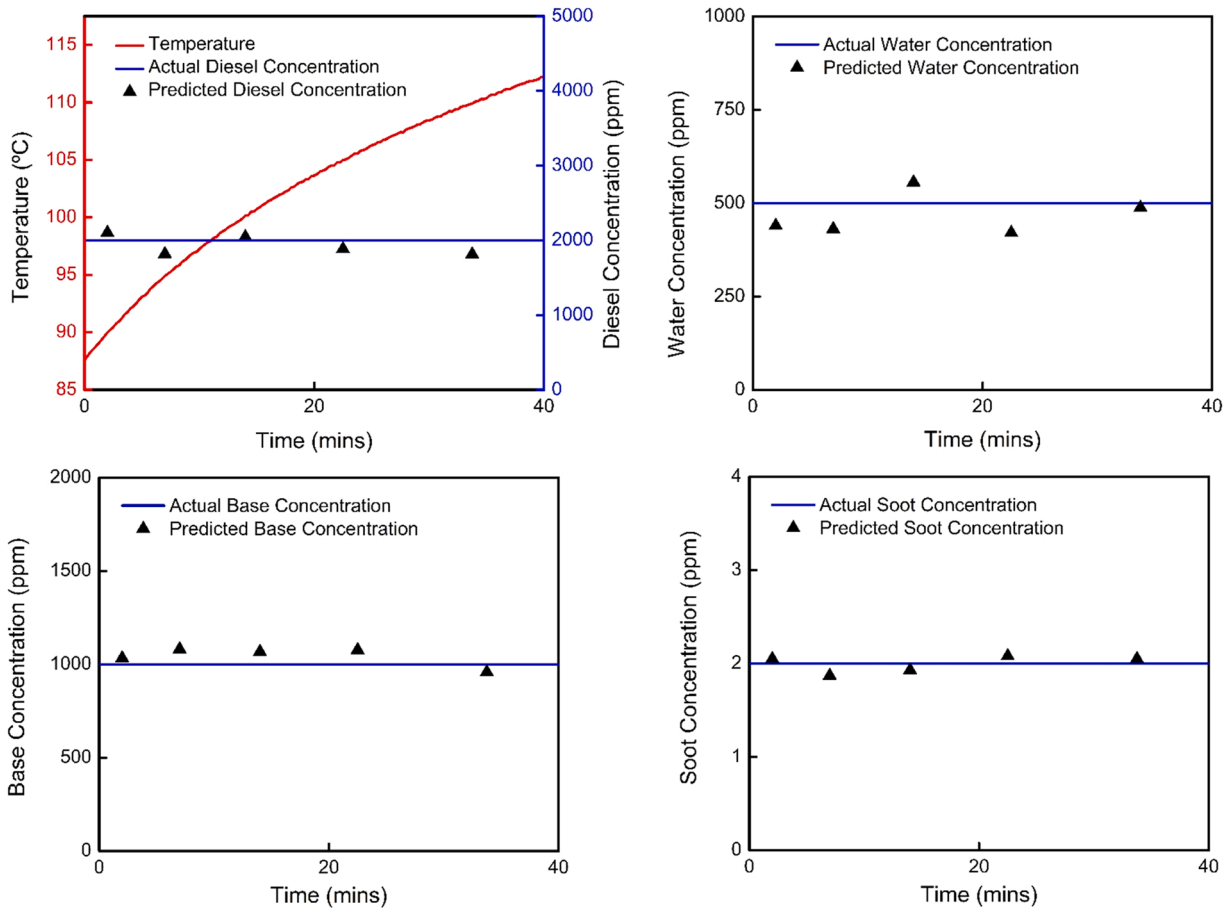

Fig. 6. Temperature variation of testing sample and predicted diesel, water, base, and soot concentration vs. time, showing that the temperature effect was removed in an environment with arbitrary temperature variations.

respectively. The average validation error at 90 ºC, 100 ºC, and 110 ºC was 5.33%, 5.68%, and 5.94% respectively. There is no consistent pattern between error and temperature or significant deviations. Based on this, the new neural network is able to effectively remove the temperature effect on property prediction.

We also compared the prediction accuracy of the neural network with and without using the deep learning techniques and SGO. Without using these techniques and using the same training and testing data sets, the average prediction accuracies were: 16.1%, 11.3%, 7.1%, and 4.2% for water, diesel, base, and soot concentrations. Apparently using the data augmentation, dropout, and SGO improves the accuracy without a need to add more datasets. This is particularly important for onsite training for online health monitoring where there is a challenge in generating a large amount of training samples onsite.

Finally, to test if the sensor array can predict the system in an environment with unstable temperatures, we selected a sample containing 2000 ppm of diesel contaminant, 500 ppm of water, 1000 ppm of base, and 2% of soot. First, the sensor array was placed into this sample for 60 min so that the sensor responses were stabilized. Next, the sample was gradually heated to mimic the arbitrary temperature change of the environment. A thermocouple (36GL12, Dayton) was used to monitor the oil temperature at real time (see Fig. 6(a), red curve). The outputs of the sensor array were recorded and analyzed using the neural network described above. Predictions on the oil's target properties were made at 9 095 100 105, and 100 ºC (see Fig. 6). In general, the predicted concentrations of target properties were in good agreement with actual concentrations. The largest error was found in water 105 ºC with an error of 15.8%, which was slightly above the maximum error of water of 15.2% in static tests (in Fig. 5). The largest errors in this test were mostly at 95 and 105 ºC, which were expected as all samples in our dataset were taken at 90 100, and 110 ºC. The results (shown in Fig. 6) show that the sensor array is able to compensate the temperature effect even in an environmental where the temperature is arbitrarily varied.

4.4. Discussion

We have developed a sensor array containing four property sensors and a thermocouple, which is utilized with an artificial neural network to accurately monitor critical properties of a lubricant oil used in a diesel-powered engine. Sensors with chemical-based sensing mechanisms are used for diesel monitoring, but they are unable to provide long term measurements. On the other hand, individual capacitive sensors which are used for monitoring these properties can suffer from cross sensitivity and provide less accurate results if another contaminant is present. The system we developed is able to monitor water, diesel fuel, base, and soot content in the oil simultaneously, live, and for extended periods of time.

The neural network architecture was uniquely selected from a simulated annealing process, which automatically searches through a range of neural network architectures to find an optimal architecture. This process helped maximize the prediction accuracy of the system to a degree not attainable through traditional methods, by overcoming local minimums and converging on a more effective architecture. The system was able to predict the water, diesel, base, and soot concentrations with an average error of 12.1%, 7.8%, 5.7%, and 3.9% respectively. This neural network had improved accuracy when compared to the predictions made using a general regression neural network (GRNN) similar to our previous work. Using the same set of data, the GRNN had average

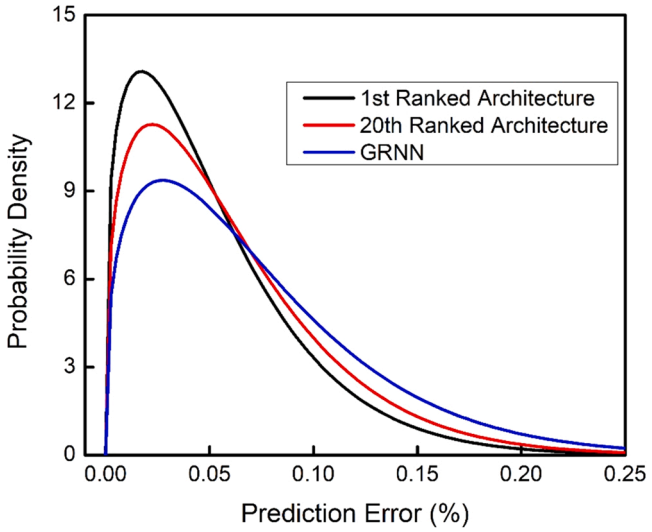

Fig. 7. Prediction error probability density for the 1st Ranked Architecture, 20th Ranked Architecture, and the GRNN.

prediction errors of 14.9%, 13.1%, 5.8%, and 6.1% for water, diesel, base, and soot respectively. The prediction errors of 3 different neural networks, 1st ranked architecture, the 20th ranked architecture, and the GRNN, were fit to Weibull distributions. The shape and scale parameters of the Weibull distribution were then used to plot each distribution to compare each network's performance (i.e. probability density at different prediction errors) [38]. Fig. 7 shows the testing data prediction error probability density of the three networks. The results clearly show that the probability density for a small prediction error was enhanced by the simulated annealing optimization, so that it was able to make more accurate predictions than the GRNN.

In addition, the temperature effect on the capacitive sensors was also removed by implementing a thermocouple to the system. Traditional temperature correction methods involve generating tedious calibration curves for a wide range of temperatures. The addition of adding a temperature measurement as an input to our neural network allows for accurate predictions at different temperatures, where our past work would need to be retrained for every temperature.

Finally, the use of data augmentation and dropout is particularly important for onsite training. New data must be collected for training for each application, since changes in the base oil and operating temperatures will affect the sensor outputs. It is impractical to gather very large amounts of data for each application, therefore it is important to use deep learning methods to counteract the negatives of a smaller dataset. Overfitting on the training set is a large issue in models with smaller datasets. Thus, applying dropout during training is of elevated importance since it reduces the effects of overfitting. Furthermore, data augmentation allows for the dataset to be artificially increased in size, alleviating the small dataset problems for onsite training.

5. Conclusions

An interdigital capacitive sensor array and artificial neural network tuned with stochastic global optimization was demonstrated for accurately measuring multiple properties of diesel powered machines. This ANN with an SGO parameter tuning process is used to untangle the overlapped responses of the sensors in the array. Simulated annealing was able to select a network architecture that had better prediction accuracy than if the architecture parameters had been selected with traditional methods. In addition, two deep learning techniques, data augmentation and dropout were used to prevent overfitting by artificially increasing the dataset and randomly disabling nodes, preventing co-adaption during training. Four critical properties: water, diesel, base, and soot concentrations were measured. Results showed that the system was able to predict the water, diesel, base, and soot concentrations with an average error of 12.1%, 7.8%, 5.7%, and 3.9% respectively, and maximum errors of 15.2%, 12.3%, 6.8%, and 6.0% respectively. Compared to general regression network, with the use of SGO, dropout, and data augmentation techniques, the accuracy of the ANN was improved. This sensing system is able to provide comprehensive information of current conditions of lubricants of a diesel powered machine, and thus provide online diagnostics and prognostics of the machine.

Funding

This material is based upon work supported by the National Science Foundation of USA under grant number PFI-TT 1940879. Any opinions, findings, and conclusions or recommendations expressed in this material are those of the author(s) and do not necessarily reflect the views of the National Science Foundation.

CRediT authorship contribution statement

Aaron Urban: Conceptualization, Software, Formal analysis, Investigation, Writing – original draft, Writing – review & editing. **Jiang Zhe:** Writing – review & editing, Supervision, Funding acquisition.

Declaration of Competing Interest

The authors declare that they have no known competing financial interests or personal relationships that could have appeared to influence the work reported in this paper.

References

[1] S. Biggs, S. Justice, Rural and agricultural mechanization: a history of the spread of small engines in selected Asian countries, IFPRI Discuss. Pap. (2015) 1–44.
[2] Karanović, V.V.; Jocanović, M.T.; Wakiru, J.M.; Orošnjak, M.D. Benefits of lubricant oil analysis for maintenance decision support: a case study. IOP Conf. Ser. Mater. Sci. Eng. 2018, 393, 012013, doi:10.1088/1757–899X/393/1/012013.
[3] X. Zhu, C. Zhong, J. Zhe, Lubricating oil conditioning sensors for online machine health monitoring – A review, Tribol. Int. 109 (2017) 473–484, https://doi.org/10.1016/J.TRIBOINT.2017.01.015.
[4] Y. Wang, Y. Chen, X. Liang, P. Tan, S. Deng, Impacts of lubricating oil and its formulations on diesel engine particle characteristics, Combust. Flame 225 (2021) 48–56, https://doi.org/10.1016/J.COMBUSTFLAME.2020.10.047.
[5] L.V. Markova, V.M. Makarenko, M.S. Semenyuk, A.P. Zozulya, On-line monitoring of the viscosity of lubricating oils, J. Frict. Wear 31 (2010) 433–442, https://doi.org/10.3103/S106836661006005X.
[6] R.E. Cantley, The effect of water in lubricating oil on bearing fatigue life, ASLE Trans. 20 (1977) 244–248, https://doi.org/10.1080/05698197708982838.
[7] A. Wolak, TBN performance study on a test fleet in real-world driving conditions using present-day engine oils, Meas. J. Int. Meas. Confed. 114 (2018) 322–331, https://doi.org/10.1016/j.measurement.2017.09.044.
[8] S. George, S. Balla, V. Gautam, M. Gautam, Effect of diesel soot on lubricant oil viscosity, Tribol. Int. 40 (2007) 809–818, https://doi.org/10.1016/j.triboint.2006.08.002.
[9] H.H. Masjuki, M.A. Maleque, The effect of palm oil diesel fuel contaminated lubricant on sliding wear of cast irons against mild steel, Wear 198 (1996) 293–299, https://doi.org/10.1016/0043-1648(96)07208-0.
[10] A. Agoston, C. Ötsch, B. Jakoby, Viscosity sensors for engine oil condition monitoring - Application and interpretation of results, Sens. Actuators A Phys. 121 (2005) 327–332, https://doi.org/10.1016/j.sna.2005.02.024.
[11] X. Zhu, L. Du, J. Zhe, An integrated lubricant oil conditioning sensor using signal multiplexing, J. Micromech. Microeng. 25 (2015), 015006, https://doi.org/10.1088/0960-1317/25/1/015006.
[12] A.J. Ricco, S.J. Martin, Acoustic wave viscosity sensor, Appl. Phys. Lett. 50 (1987) 1474–1476, https://doi.org/10.1063/1.97804.
[13] X. Zhu, L. Du, B. Liu, J. Zhe, A microsensor array for quantification of lubricant contaminants using a back propagation artificial neural network, J. Micromech. Microeng. 26 (2016), 065005, https://doi.org/10.1088/0960-1317/26/6/065005.
[14] D. Jiao, A. Urban, X. Zhu, J. Zhe, Oil property sensing array based on a general regression neural network, Tribol. Int. 164 (2021), 107221, https://doi.org/10.1016/J.TRIBOINT.2021.107221.
[15] W.A. Altabey, The thermal effect on electrical capacitance sensor for two-phase flow monitoring, Struct. Monit. Maint. 3 (2016) 335–347, https://doi.org/10.12989/smm.2016.3.4.335.

[16] A.H. Jayatissa, Z. Li, Effect of temperature on capacitance-voltage characteristics of SOI. Mater. Sci. Eng. B Solid-State Mater, Adv. Technol. 124–125 (2005) 331–334, https://doi.org/10.1016/j.mseb.2005.08.041.
[17] A.Y. El-Naggar, R.A. El-Adly, T.A. Altalhi, A. Alhadhrami, F. Modather, M.A. Ebiad, A. Salem, Oxidation stability of lubricating base oils, Pet. Sci. Technol. 36 (2018) 179–185, https://doi.org/10.1080/10916466.2017.1403450.
[18] Fabian, Z.; Heckel, R.; Soltanolkotabi, M. Data augmentation for deep learning based accelerated MRI reconstruction with limited data. *Proc. 38th Int. Conf. Mach. Learn.* 2021.
[19] L. Huang, W. Pan, Y. Zhang, L. Qian, N. Gao, Y. Wu, Data augmentation for deep learning-based radio modulation classification, IEEE Access 8 (2020) 1498–1506, doi:10.1109/ACCESS.2019.2960775.
[20] E. Lashgari, D. Liang, U. Maoz, Data augmentation for deep-learning-based electroencephalography, J. Neurosci. Methods 346 (2020), 108885, https://doi.org/10.1016/j.jneumeth.2020.108885.
[21] N. Srivastava, G. Hinton, A. Krizhevsky, I. Sutskever, R. Salakhutdinov, Dropout: a simple way to prevent neural networks from overfitting, 15 1929-1958, J. Mach. Learn. Res. 15 (2014) 1929–1958, https://doi.org/10.1016/0370-2693(93)90272-J.
[22] A. Niimi, Deep learning for credit card data analysis. 2015 World Congr, Internet Secur. World 2015 (2015) 73–77, https://doi.org/10.1109/WorldCIS.2015.7359417.
[23] N. Munir, H.J. Kim, S.J. Song, S.S. Kang, Investigation of deep neural network with drop out for ultrasonic flaw classification in weldments, J. Mech. Sci. Technol. 32 (2018) 3073–3080, https://doi.org/10.1007/s12206-018-0610-1.
[24] X. Zhu, L. Du, J. Zhe, An integrated lubricant oil conditioning sensor using signal multiplexing, J. Micromech. Microeng. 25 (2014) 15006, https://doi.org/10.1088/0960-1317/25/1/015006.
[25] U. Kang, K.D. Wise, A high-speed capacitive humidity sensor with on-chip thermal reset, 702–170, IEEE Trans. Electron Devices 47 (2000), https://doi.org/10.1109/16.830983.
[26] Laconte, J.; Wilmart, V.; Flandre, D.; Raskin, J.P. High-Sensitivity Capacitive Humidity Sensor Using 3-Layer Patterned Polyimide Sensing Film. In Proceedings of the Proceedings of IEEE Sensors; 2003; p. 372.
[27] M. Ercelik, A. Ozden, Y. Devrim, C.O. Colpan, Investigation of Nafion based composite membranes on the performance of DMFCs, Int. J. Hydrog. Energy 42 (2017) 2658–2668, https://doi.org/10.1016/j.ijhydene.2016.06.215.
[28] S. Capone, M. Zuppa, D.S. Presicce, L. Francioso, F. Casino, P. Siciliano, Metal oxide gas sensor array for the detection of diesel fuel in engine oil, Sens. Actuators, B Chem. 131 (2008) 125–133, https://doi.org/10.1016/j.snb.2007.12.029.
[29] M.F. Smiechowski, V.F. Lvovich, Electrochemical monitoring of water-surfactant interactions in industrial lubricants, J. Electroanal. Chem. (2002), https://doi.org/10.1016/S0022-0728(02)01106-3.
[30] CIMAC Guidelines for Diesel Engines lubrication, Oil degradation. Int. Counc. Combust. Engines 2004, 66.
[31] V. Çelik, E. Arcaklioğlu, Performance maps of a diesel engine, Appl. Energy 81 (2005) 247–259, https://doi.org/10.1016/j.apenergy.2004.08.003.
[32] A. Zhigljavsky, A. Zilinskas, Stochastic Global Optimization, Vol. 9, Springer Science & Business Media, 2007.
[33] H.E. Romeijn, R.L. Smith, Simulated annealing for constrained global optimization, J. Glob. Optim. 5 (1994) 101–126, https://doi.org/10.1007/BF01100688.
[34] Michel Gendreau, J. -Y. P. Handb. Metaheuristic Vol. 272 (2019). ISBN 9783319910857.
[35] Vujičić, T.; Matijevi, T. Comparative Analysis of Methods for Determining Number of Hidden Neurons in Artificial Neural Network. Cent. Eur. Conf. Inf. Intell. Syst. 2016, 219–223.
[36] Demuth, H.; Beale, M. Neural Network Toolbox For Use with MATLAB Available online: http://cda.psych.uiuc.edu/matlab_pdf/nnet.pdf (accessed on May 24, 2021).
[37] E. Bechhoefer, J. Zhu, D. He, Survey of lubrication oil condition monitoring, diagnostics, prognostics techniques and systems Related papers Lubricat ion oil condit ion monit oring and remaining useful life predict ion wit h part icle filt ering Eric Bechhoefer a review on comparison, J. Chem. Sci. Technol. 2 (2013) 100–115.
[38] R.H. Kushler, Comput. Stat. Handb. MATLAB ® 44 (2002). ISBN 1584882298.

Aaron William Urban received his B.S. in Mechanical Engineering from The University of Akron in 2019. He is currently a mechanical engineering master's student at The University of Akron. His areas of research include micro devices, capacitive and inductive sensors, measurement systems, and artificial neural networks.

Jiang Zhe received M. Phil. and Ph.D. degrees from Columbia University in 2000 and 2002, respectively. From 2001–2002, he was a MEMS engineer with Fitel Technologies, Inc., and he was a MEMS development engineer for Advanced Microsensors Inc. in 2002. He joined the University of Akron in 2003, where he serves as Professor of Mechanical Engineering. His research interests include micro and nano sensors, biosensors and bioinstruments, lab on a chip, microfluidic and nanofluidic devices, machine health monitoring, and artificial neural networks for sensor networks. Dr. Zhe is a member of the American Society of Mechanical Engineers.